Structural and chemical analysis of TiO2 nanotube surface for dye-sensitized solar cells

Structural and chemical analysis of TiO_2 nanotube surface for dye-sensitized solar cells

Raimu Endo [a], Hirulak. D. Siriwardena [b], Atsuyoshi Kondo [a], Chisato Yamamoto [a], Masaru Shimomura [a,b,]*

[a] Graduate School of Integrated Science & Technology, Shizuoka University, 3-5-1 Johoku, Nakaku 432-8561, Hamamatsu, Shizuoka, Japan.

[b] Graduate School of Science & Technology, Shizuoka University, 3-5-1 Johoku, Nakaku 432-8011, Hamamatsu, Shizuoka, Japan

Abstract

One-dimensional TiO_2 nanotube (TNT) arrays were fabricated on fluorine-doped tin oxide glass substrate as the photoanodes for dye-sensitized solar cells (DSCs) using one-step ZnO nanorods template method. The depth profile analysis using X-ray photoelectron spectroscopy and ion sputtering indicated that a small amount of Zn species was attached on the TNT surface. Relationship of the properties of the TNT surface with the Zn residue and the photovoltaic characteristics of DSCs were investigated. Residual Zn species on TNT improve the open circuit voltage of the DSCs. A maximum open circuit voltage of 0.876 V was achieved, which is close to the theoretical maximum of the TiO_2-based DSCs. However, photocurrent density was decreased significantly for the high-Zn-amount sample. It was revealed that the surface Zn species were divalent oxides and the amount of surface hydroxyl group was increased in conjunction with the Zn amount. Slight increase of the dye amount was found for the high Zn amount sample. It was expected that decrease in injection probability of the photo-excited electrons into TNT was the dominant reason for the photocurrent decrease.

Graphical abstract

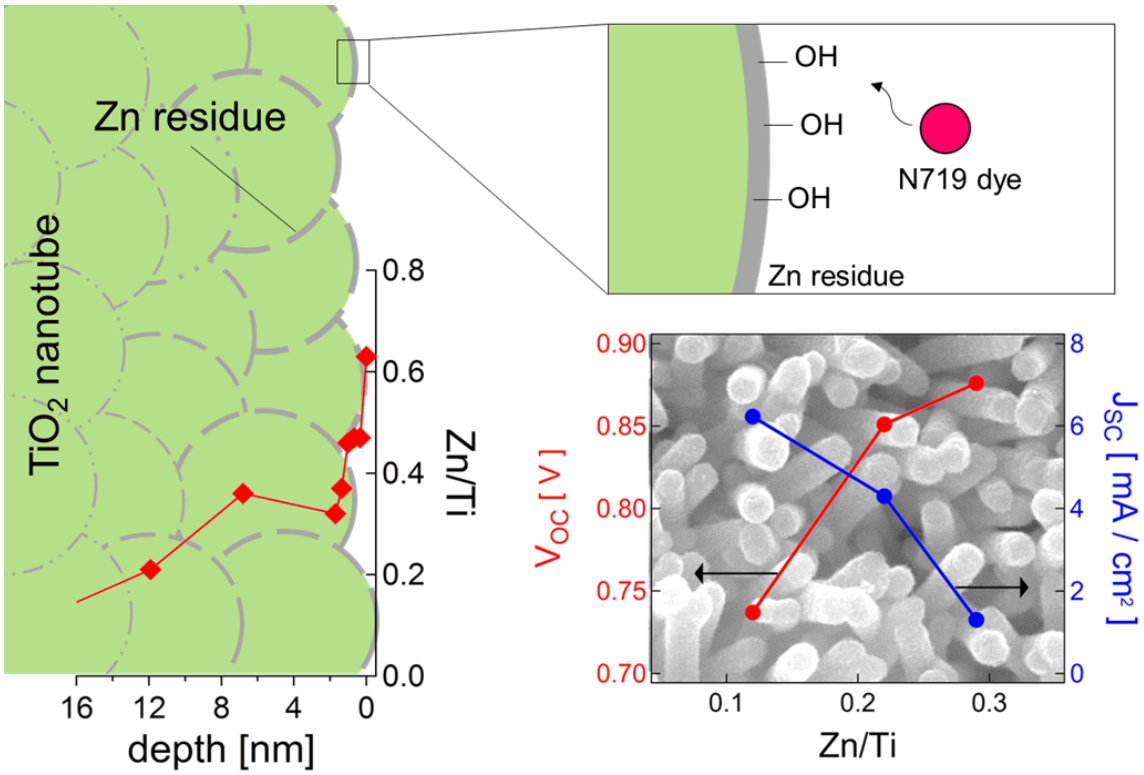

Abbreviations

TNT, titanium dioxide nanotube; ZNR, zinc oxide nanorod; DSC, dye-sensitized solar cell; FTO, fluorine doped tin oxide; AHFT, ammonium hexafluoro titanate; LPD, liquid phase deposition; Ar-GCIB, argon gas cluster ion beam; HZC, high zinc concentration; MZC, middle zinc concentration; LZC, low zinc concentration

Keywords

TiO_2 nanotubes; ZnO nanorods; Dye-sensitized solar cells; Photoanode; X-ray photoelectron spectroscopy

1. Introduction

Solar energy is one of the most promising sources of energy and has the potential to provide solutions for the current energy crisis. Dye-sensitized solar cells (DSCs) are inexpensive and versatile alternatives to convert solar energy to electrical energy [1]. The most studied DSC contains a ruthenium-based dye adsorbed onto a layer of interconnected TiO_2 nanoparticles deposited on a fluorine-doped tin-oxide-coated glass (FTO) as the working electrode, with lightly platinised FTO as the counter electrode and a liquid electrolyte having I^-/I_3^- sandwiched between the two electrodes.

The solar energy conversion efficiency of DSC is determined by the product of the open-circuit voltage (V_{OC}), short-circuit current density (J_{SC}), and fill factor (FF). V_{OC} of DSC is determined by the energy difference between the quasi-Fermi level of the TiO_2 and the I^-/I_3^- redox potential in the electrolyte. The efficiency of the TiO_2-based DSCs has been limited owing to the maximum diffusion length of an electron in the TiO_2 network [2][3]. The photo-generated electrons transport in a randomly oriented TiO_2 nanoparticle network via diffusion with many trapping and de-trapping processes [4]. This process decelerates the flow of photo-electrons, increasing the recombination with oxidised dye molecules and I_3^- at the TiO_2 particle boundaries [5]. When electrons are trapped by numerous surface states existing on the surface, the quasi-Fermi level of TiO_2 and the V_{OC} obtained decrease.

One-dimensional (1D) TiO_2 nanostructures can be used to replace TiO_2 nanoparticle networks in DSCs to avoid this random walk problem [6]. Accordingly, TiO_2 1D structures such as nanotubes [7][8][9] and nanorods [10][11][12] have been used. The use of TiO_2 1D structures reduces the number of boundaries to be passed by a photo-exited electron, providing a direct path to the FTO substrate [13][14]. Furthermore, light scattering and light harvesting can also be improved [15].

Anodic oxidation of titanium metal in an electrolyte containing fluoride is the most common technique used to prepare TiO_2 1D nanostructures [16][17]. There are numerous other methods of preparing TiO_2 1D structures such as sol-gel techniques [18][19] and hydrothermal techniques [20]. Although TiO_2 1D nanostructures can be fabricated using these techniques, high efficiencies can only be expected from nanotubes vertically aligned to the conducting substrate. Nevertheless, DSCs based on TiO_2 1D nanostructures have not exhibited a significant increase in efficiency as expected. Comparably, TiO_2 nanotube (TNT) arrays have limited surface area for dye loading and therefore, the photocurrent of the device is also small, yielding lower efficiencies.

In contrast to conventional anodisation methods, the preparation of TNT arrays using a template-assisted technique is an easy, effective, and inexpensive method [21]. In this study, a template-assisted one-step synthesis process is used for the fabrication of TNT arrays with different lengths. Vertically aligned ZnO nanorod (ZNR) arrays—prepared using the aqueous solution method at low temperature—are used as the template, and the formation of TNT and template etching of ZNR occur simultaneously. ZNR arrays are used as the template because they can be grown at low temperature and can grow continuously [22][23][24][25][26]. Liquid phase deposition (LPD) process [21], which is used to deposit TiO_2, has several benefits over other deposition techniques. TiO_2 can be deposited at room temperature (~300 K) by simply immersing the template in the solution mixture. As the deposition of a metal oxide thin film occurs via a chemical equilibrium reaction between the metal fluoride complex and metal oxide, homogenous and thickness-controllable films can be deposited on substrates with complex and larger surface areas [27]. The length and diameter of the ZNR template were controlled by changing the duration of growth time. The fabricated TNT reflects the shape of the ZNR template and has a hollow shape with its top capped. The surface effects are predominant in

this system as the TNT arrays are formed owing to the deposition of TiO_2 nanoparticles on the ZNR template.

In the LPD method, a small amount of Zn species derived from the template can remain on the TNT surface because the dissolution of ZNR template and the deposition of TiO_2 occur simultaneously. As mentioned earlier, these TNT arrays are formed with TiO_2 nanoparticles and are significantly influenced by their surface structure when used as a photoanode for DSCs. It has been reported that the DSC performance changes significantly owing to the existence of a small amount of element on the surface of the TiO_2 photoanode [28][29][30]. Therefore, the influence of the residual Zn on the TNT surface cannot be ignored.

DSCs were fabricated using TiO_2 1-D nanostructures with different lengths, and the effect on the efficiency of the device was investigated. Furthermore, the residual amount of Zn was also varied, and the influence of the photovoltaic parameters was observed.

2. Experimental

2.1.Preparation of TNT arrays

In order to fabricate the ZNR template, ZnO seed layers were prepared by spin coating of an ethanolic seed layer solution on thoroughly cleaned FTO plates. The seed layer solution was prepared by dissolving 0.2 M $Zn(CH_3COO)_2 \cdot 2H_2O$ (Wako, 99.0%) and 0.2 M 2,2'-Iminodiethanol (DEA, Wako, 99.0%) in ethanol. The plates were subsequently baked at 100 °C for 10 min, and this step was repeated three times in order to obtain a uniform seed layer. These seeded FTO plates were subsequently annealed at 350 °C for 1 h [31]. Subsequently, the seeded FTO plates were cooled down to room temperature and suspended in an aqueous solution of 0.02 M $Zn(NO_3)_2 \cdot 6H_2O$ (Wako, 99.0%) and 0.02 M hexamethylenetetramine (Wako, 99.0%) for 3 h at 90 °C. The solution mixture was changed every 3 h and the process was carried out for 9 h [22]. One three-hour period was considered as a growth process, and three growth

processes were carried out in total. The plates were removed after the growth process, washed with distilled water, and dried in air. In order to prepare TNT arrays, the template was suspended in a solution containing 0.05 M $(NH_4)_2TiF_6$ (AHFT, Aldrich, 99.99%) and 0.15 M boric acid (Wako, 99.5%) at room temperature for 3 h [21]. FTO plates with TNT arrays were removed from the solution after the LPD, allowed to dry in air, and annealed at 500 °C for 30 min.

Samples prepared after three ZNR template growth processes were used to investigate the effects of the surface residual Zn on the TNT arrays and photovoltaic properties of DSCs fabricated using these TNT arrays. The amount of residual Zn was controlled by changing the volume of the AHFT and boric acid solution (10, 30, and 60 mL) in the TiO_2 deposition and ZnO dissolution phase.

2.2. Fabrication of DSCs

Cells prepared with the TNT arrays were immersed in a 0.3 mM N719 ruthenium dye (Solaronix S.A.) solution for 20 h and used as the working electrode to fabricate DSCs. An electrolyte containing I^-/I_3^- redox couple (0.39 M 1,2-dimethyl-3-propylimidazolium iodide (Wako), 0.064 M lithium iodide (Wako), 0.17 M 4-tert-butyl-pyridine (TCI chemicals), 0.065 M iodine (Wako), and 0.12 M guanidine thiocyanate (Wako) dissolved in acetonitrile (Wako) was sandwiched between the working electrode and lightly platinised FTO counter electrode. The *I–V* characteristics of the fabricated DSCs were subsequently determined by using a JASCO CEP-25BX solar simulator.

2.3. Characterisation

The fabricated TNT samples were characterised by using field-emission scanning electron microscope (FE-SEM, JEOL, JSM-6320F, JSM-7001F), X-ray diffractometer (XRD, Rigaku,

RINT-Ultima Ⅲ), and transmission electron microscope (TEM, JEOL, JEM-2000RX Ⅱ). X-ray photoelectron spectroscopy (XPS, SHIMADZU, AXIS ULTRA DLD) analysis was carried out for TNT samples with different amounts of surface Zn residues using a monochromated Al K α source.

In the XPS analysis, the standard Shirley approach was adopted for the background subtraction, and the Voigt function was used for the curve fitting of the XPS spectra. The peak of the surface-contaminated carbon was shifted to 285.00 eV to neutralise the charging occurring during the XPS measurements. The TNT arrays obtained after a single growth process were etched using an argon gas cluster ion beam (Ar-GCIB) to identify the depth direction of the surface Zn residues. The Ar-GCIB was irradiated at an accelerating voltage of 5 kV, and the sputtering range was fixed at 1 × 1 mm^2. The gas cluster contained Ar 1000^+ atoms and sputtering was carried out for 100 min. The XPS data were obtained at certain time intervals during the sputtering process.

In order to compare the dye adsorption capabilities of different samples, adsorbed dye on an area of 1.5 cm^2 was desorbed into 4 mL of 0.05 M NaOH solution, and adsorption measurements were carried out using a UV–Vis spectrometer (SHIMADZU, UV-3100PC).

3. Results and discussion

3.1. Characterisation of the TNT arrays of different lengths

The wurtzite crystal structure of ZnO exhibited partial polar characteristics and the (001) plane of the structure was the basal polar plane. The opposite ends of the basal polar plane had partially positive Zn lattice points and partially negative oxygen lattice points as shown in Figure 1(a). Hexamethylenetetramine preferentially became attached to the non-polar facets of the ZNR as a non-polar chelating agent, exposing only the (001) plane [32]. Moreover, the (001) plane exhibited a lower surface free energy of 1.6 J/m^2, when compared to the (100) and

(101) planes, which had surface free energies of 3.4 J/m^2 and 2.0 J/m^2, respectively [22]. These facts contributed to the prominent and continuous epitaxial growth along the (001) direction, as shown in Figure 1(b), resulting in longer ZNR when the growth process was continued by replacing the reaction mixture.

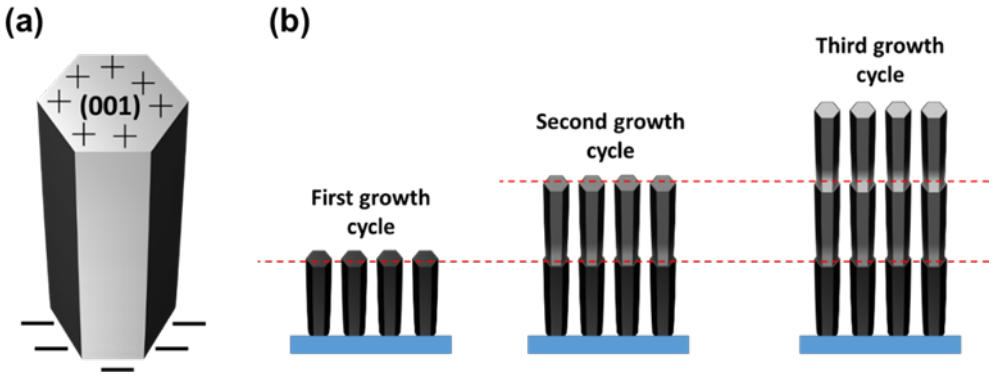

Figure 1 (a) Partial polar characteristics of ZnO wurtzite structure and (b) the growth process of the ZNR template in each growth cycle

Figure 2(a)–(c) show the SEM images of the ZNR templates obtained after one growth cycle (1GC), two growth cycles (2GC), and three growth cycles (3GC), respectively. ZNR templates with the average lengths of 0.7, 1.6, and 3.0 μm were obtained by increasing the reaction time and replacing the reaction mixture. The continuous growth process increased the length of the ZNR templates.

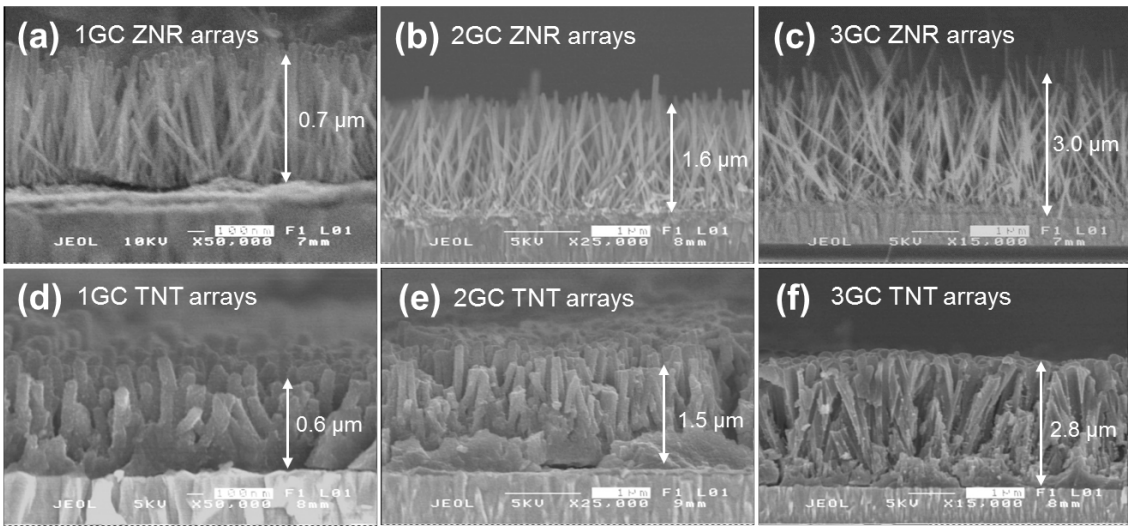

Figure 2 Cross-sectional SEM images of ZnO nanorod arrays and TiO_2 nanotube arrays of (a)(d) 1GC, (b)(e) 2GC, and (c)(f) 3GC

TiO_2 was believed to be deposited via the ligand-exchange reaction of metal-fluoro complex ion and the reaction of F^- ion with boric acid. The following equilibrium reaction is proposed for the metal-fluoro complex in the reaction mixture [33].

$$TiF_6^{2-} + 2H_2O \leftrightharpoons TiO_2 + 6F^- + 4H^+ \quad (1)$$

Boric acid acted as a F^- scavenger, thus shifting the equilibrium reaction (1) to the right-hand side, forming more stable complex ions.

$$H_3BO_3 + 4H^+ + 4F^- \leftrightharpoons BF_4^- + H_3O^+ + 2H_2O \quad (2)$$

Moreover, the additional boric acid in the solution contributed to the etching process of the ZNR template, which was covered with a thin layer of TiO_2 nanoparticles, forming a ZnO/TiO_2 core-shell structure, as shown in equation (3).

$$ZnO + 2H^+ \rightarrow Zn^{2+} + H_2O \quad (3)$$

The SEM images of the TNT arrays obtained using the ZNR templates after each growth process are shown in Figure 2(d)–(f). The diameter of the ZNR templates increased when the reaction time was extended in the growth process. Therefore, an increase in the diameter of

TNT arrays was also observed when the corresponding ZNR templates were used. The diameter of TNT arrays varies in the range of 80–200 nm, which was confirmed by the TEM analysis. As the deposition time of TiO_2 was constant (3 h) regardless of the length of the ZNR template, the average wall thickness of TNT remained fixed at approximately 30 nm in every situation. The TNT arrays were formed with nanoparticles of size 5–15 nm as shown in Figure 3, which can be attributed to the large surface area. This can be advantageous in the dye adsorption process. Although TNT had a hollow structure, the inner wall could not be utilised for dye adsorption as TNT was capped at the end, which is a disadvantage. As TiO_2 precipitated on the entire surface of the ZNR template during the TiO_2 deposition process, it was difficult to develop TNT with an open upper end. The dye adsorption could be improved by removing the upper end cap of TNT by using a glycerol solution with a small amount of HF and water [34].

The average length of TNT was approximately 2.8 μm. It was 200 nm shorter than that of the template owing to the fast etching process of the template. The formation of TNT arrays and dissolution of ZNR template occurred simultaneously when the LPD method was used. This may be the reason for the difference between the lengths of the template and TNT arrays. A longer deposition time provides TNTs with a thicker outer shell.

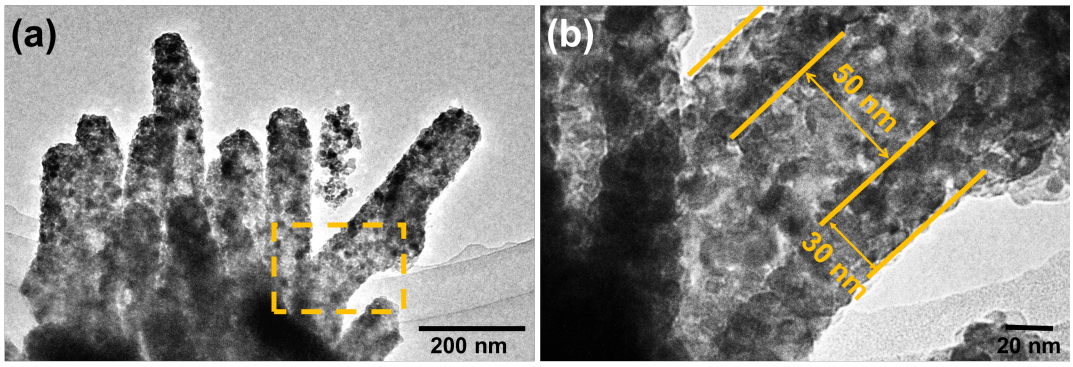

Figure 3 TEM images of the TNT after 3GC. The area indicated by the square in (a) is magnified and shown in (b) with the corresponding dimensions of the TNT.

The photovoltaic characteristics of the DSCs fabricated using N719 dye-adsorbed TNT arrays with different lengths (0.6, 1.5, and 2.8 μm) are listed in Table 1 and the corresponding *I–V* curves are shown in Figure 4(a). (Used TNT samples are denoted as LZC (low zinc concentration) as the residual Zn amounts on the surface were small, which was confirmed by XPS measurement.) It can be clearly observed that the efficiency of the DSCs increased significantly when the photoanode was fabricated with longer TNT arrays. A power conversion efficiency of 3.62% was obtained for the DSCs prepared using TNT arrays with an average length of 2.8 μm. This is an impressive result as the average film thickness of the photoanode was only 2.8 μm. A higher surface area was available when longer TNT arrays were used, thus enhancing the photocurrent. Moreover, as mentioned above, TNT arrays were formed owing to the deposition of TiO_2 nanoparticles on the template. Therefore, the TNT system had higher surface energy compared to other systems, allowing more dye molecules to become attached to the surface and fully exploiting the available surface area. Conventional DSCs fabricated with TiO_2 nanoparticles are invisible to light, and therefore, they cannot effectively utilise the incident light. The use of 1-D nanostructures prevents this problem by enhancing the light scattering effect and allowing the dye molecules to fully utilise the incident light. Longer TNT

arrays increase the light scattering effect and this improvement in light harvesting property may also have contributed to the higher photocurrent.

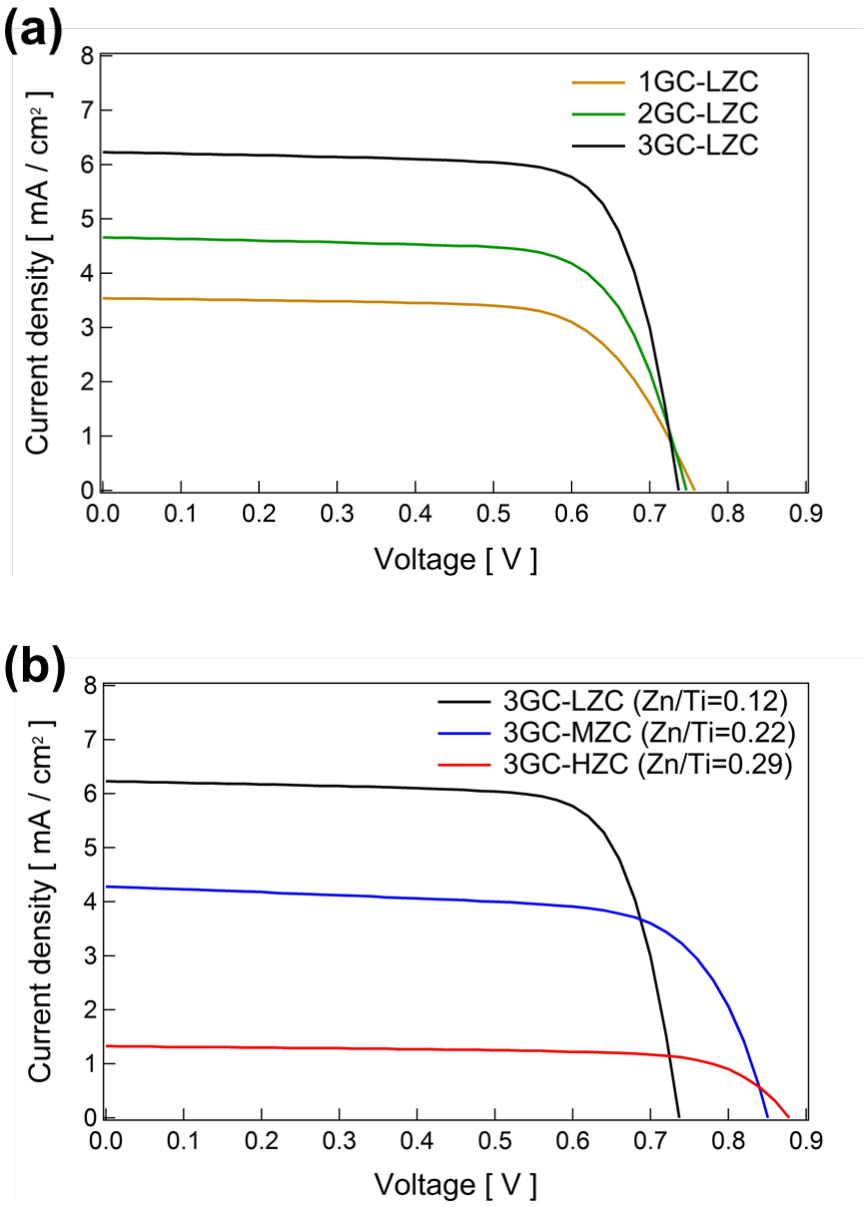

Figure 4 *I–V* characteristic curves of DSCs fabricated using TNT arrays of (a) 1 to 3GC with low zinc concentration (1GC-LZC, 2GC-LZC, 3GC-LZC) and (b) 3GC samples with low, middle, and high zinc concentration (3GC-LZC, 3GC-MZC, 3GC-HZC), measured under AM-1.5 illumination.

Table 1 Photovoltaic parameters of the DSCs fabricated using the TNT arrays of (a) 1 to 3GC with low zinc concentration (1GC-LZC, 2GC-LZC, 3GC-LZC) and (b) 3GC samples with low, middle, and high zinc concentration (3GC-LZC, 3GC-MZC, 3GC-HZC).

Sample	J_{SC} [mA/cm²]	V_{OC} [V]	FF [-]	Efficiency [%]
1GC-LZC	3.54	0.758	0.700	1.86
2GC-LZC	4.67	0.747	0.751	2.51
3GC-LZC	6.23	0.737	0.754	3.62
3GC-MZC	4.30	0.851	0.692	2.52
3GC-HZC	1.30	0.876	0.711	0.83

3.2. Effect of the amount of surface Zn species on the electronic states and photovoltaic characteristics

Zn species can exist on the TNT arrays prepared using the one-step template method owing to the TiO_2 deposition/ZnO dissolution reactions. The existence of the surface Zn residue was confirmed using the XPS data. These Zn residues on the TNT surface were formed as a result of the ZNR dissolution reaction. In order to investigate the distribution of the surface Zn residues, a depth direction analysis was performed on the TNT arrays fabricated with 1GC ZNR template via the GCIB of Ar 1000^+ atoms. During the measurement, an angle of 45° was maintained between the sample surface and Ar-GCIB. Before the etching process was started, 1.3% of the surface Zn residue (Zn/Ti=0.063) was observed on the TNT array surface of 1GC-LZC, which was fabricated in 60 mL AHFT and boric acid solution. As the etching with Ar-GCIB progressed, the intensity of the Zn 2p peak decreased and the peak completely disappeared after 40–70 min of etching, as shown in Figure 5(a). Figure 5(b) illustrates the plots of the atomic ratio of Zn/Ti as a function of the depth from the TNT surface. The depth

was calculated using the etching rate correlation on a SiO_2 film (0.17 nm/min) and most of the Zn residue was expected to exist at approximately 3.3 nm from the TNT surface.

The amount of surface Zn residue on the TNTs was controlled by varying the volume of the reaction solution containing AHFT and boric acid. As shown in chemical equation (3), during the TiO_2 deposition and ZNR template dissolution reaction, Zn^{2+} ions were released into the reaction solution. The growth area of the ZNR template on the FTO substrate was maintained constant (1.5 cm^2), and different volumes (10, 30, and 60 mL) of the reaction mixture were used. Therefore, different amounts of Zn residues remained on the surface of TNTs. The XPS composition analysis of the TNT arrays obtained by changing the volume of the AHFT and boric acid solution mixture is shown in Figure 6. The data obtained from the XPS spectra are listed in Table 2, and it was observed that the amount of surface Zn residue increased when the volume of the AHFT and boric acid reaction mixture decreased. The atomic ratio of Zn/Ti were determined to 0.12, 0.22, and 0.29 for the three different volumes of the solution.

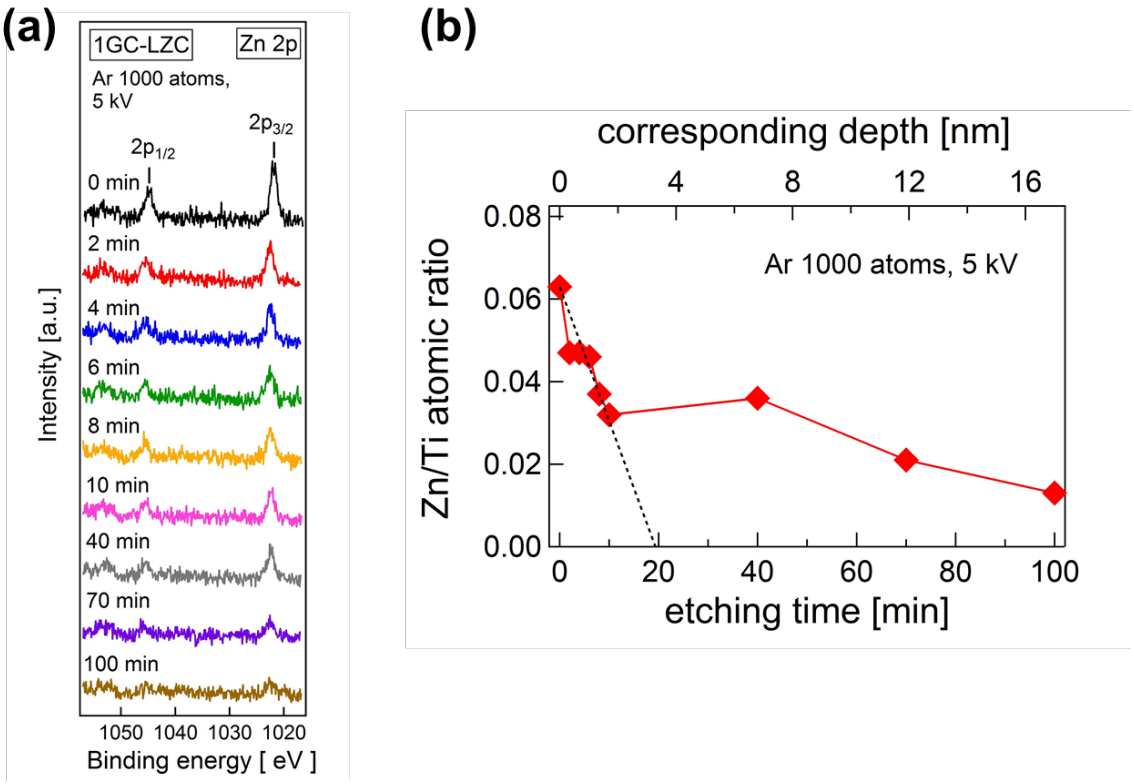

Figure 5 (a) XPS of Zn 2p narrow spectra (b) the corresponding depth profile of Zn/Ti atomic ratio for the TNT arrays of 1GC-LZC obtained at different sputtering times. Sputtering conditions were Ar cluster size of 1000, an acceleration voltage of 5 kV, and an irradiation area of 1×1 mm^2 .

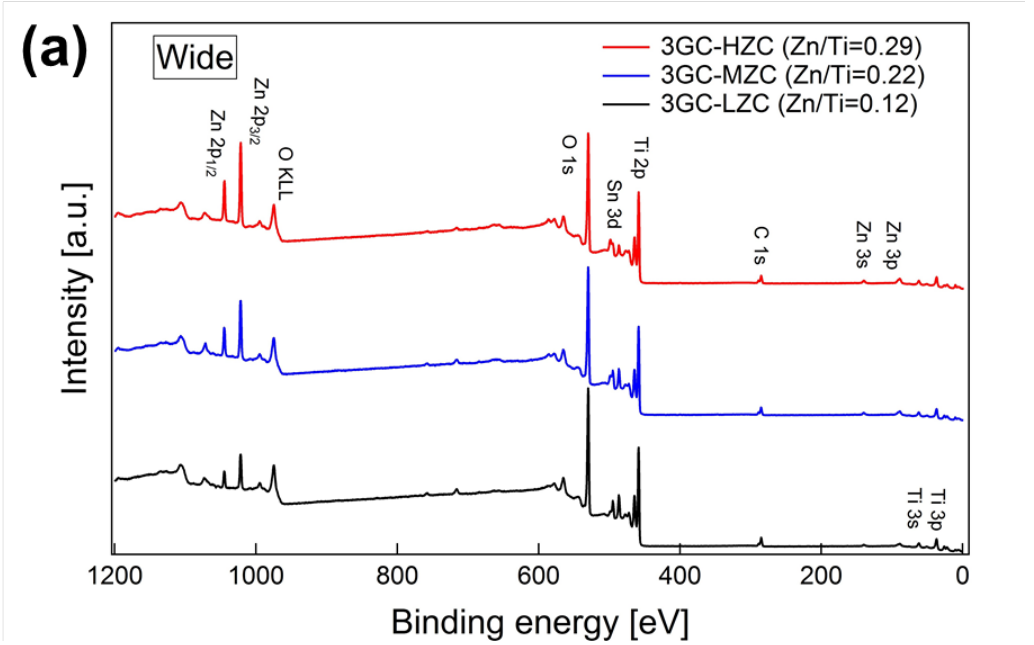
(a)
Wide
3GC-HZC (Zn/Ti=0.29)
3GC-MZC (Zn/Ti=0.22)
3GC-LZC (Zn/Ti=0.12)
Zn 2p1/2
Zn 2p3/2
O KLL
O 1s
Ti 2p
Sn 3d
C 1s
Zn 3s
Zn 3p
Ti 3p
Ti 3s
Intensity [a.u.]
1200
1000
800
600
400
200
0
Binding energy [eV]

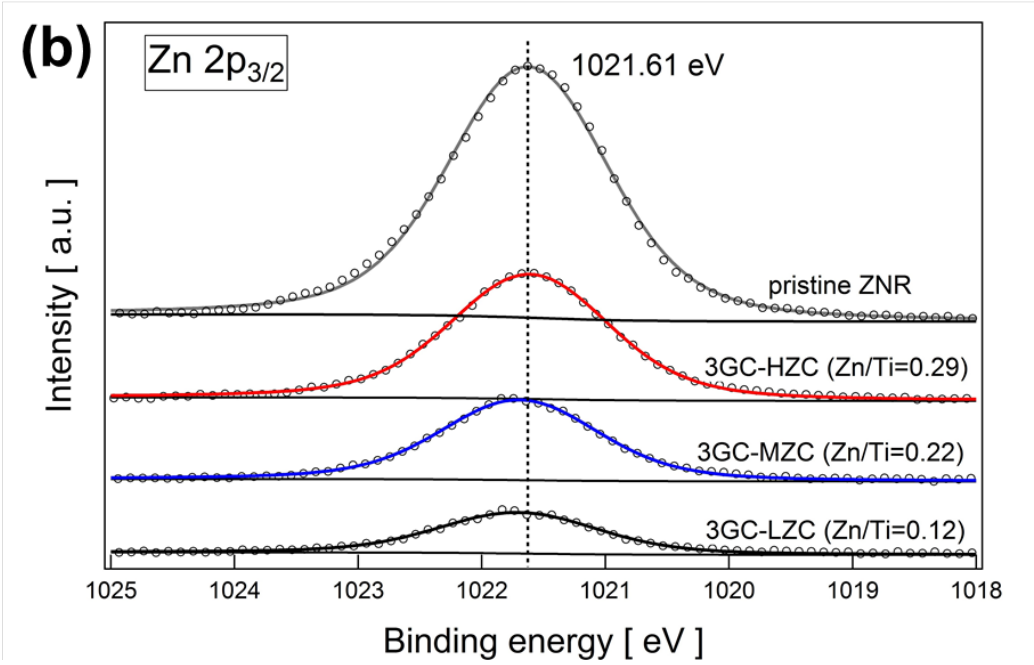
(b)
Zn 2p3/2
1021.61 eV
pristine ZNR
3GC-HZC (Zn/Ti=0.29)
3GC-MZC (Zn/Ti=0.22)
3GC-LZC (Zn/Ti=0.12)
Intensity [a.u.]
1025
1024
1023
1022
1021
1020
1019
1018
Binding energy [eV]

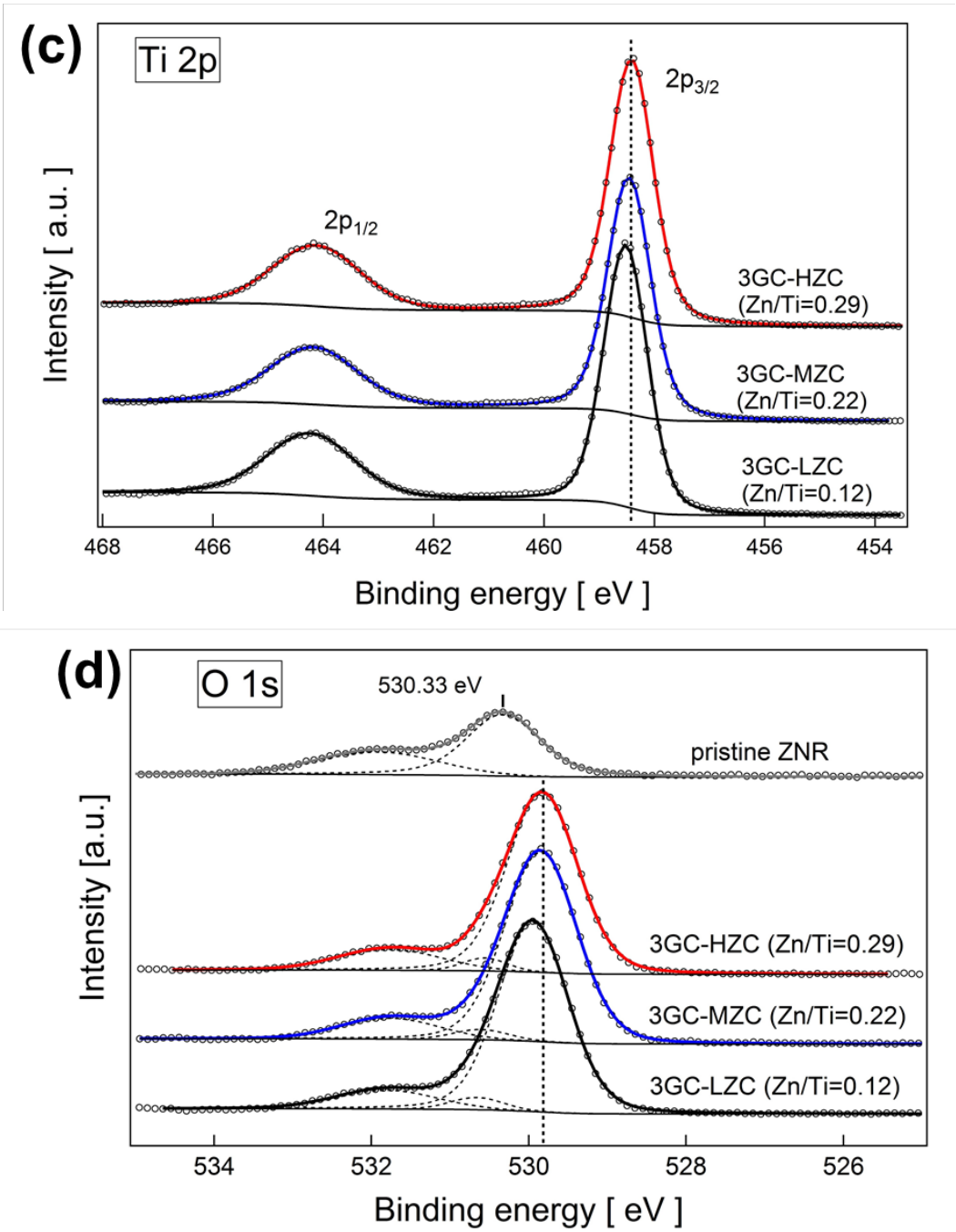

Figure 6 (a) XPS wide spectra, (b) Zn 2p, (c) Ti 2p, and (d) O 1s narrow spectra of the TNT 3GC-HZC, 3GC-MZC, 3GC-LZC. (c) and (d) show the Zn 2p and O 1s narrow spectra of pristine ZnO nanorod arrays, respectively.

Table 2 Surface elemental composition of 3GC TNT arrays.

Sample	Atomic concentration [%]						Zn/Ti atomic ratio
	Ti	Zn	O	C	Sn	Total	
3GC-HZC	19.7	5.7	60.3	13.4	0.8	100	0.29
3GC-MZC	19.9	4.4	60.6	13.6	1.6	100	0.22
3GC-LZC	21.3	2.5	60.6	13.7	1.9	100	0.12

However, as shown in Figure 7, the XRD analysis of the TNT samples with various amounts of the surface Zn residue only revealed peaks corresponding to the FTO substrate and anatase TiO_2. The XRD peaks derived from ZnO or $ZnTiO_3$ were not observed even for the samples with a high amount of surface Zn residue. It can be concluded that the amount of residual Zn was low and localised on the TNT surface, and the ZNR template dissolved almost completely. The amount of Zn available on the TNT surface was below the detection sensitivity of the XRD as it is a bulk-sensitive technique. However, a significant amount of surface Zn was available and could only be detected by a sensitive measurement method such as XPS.

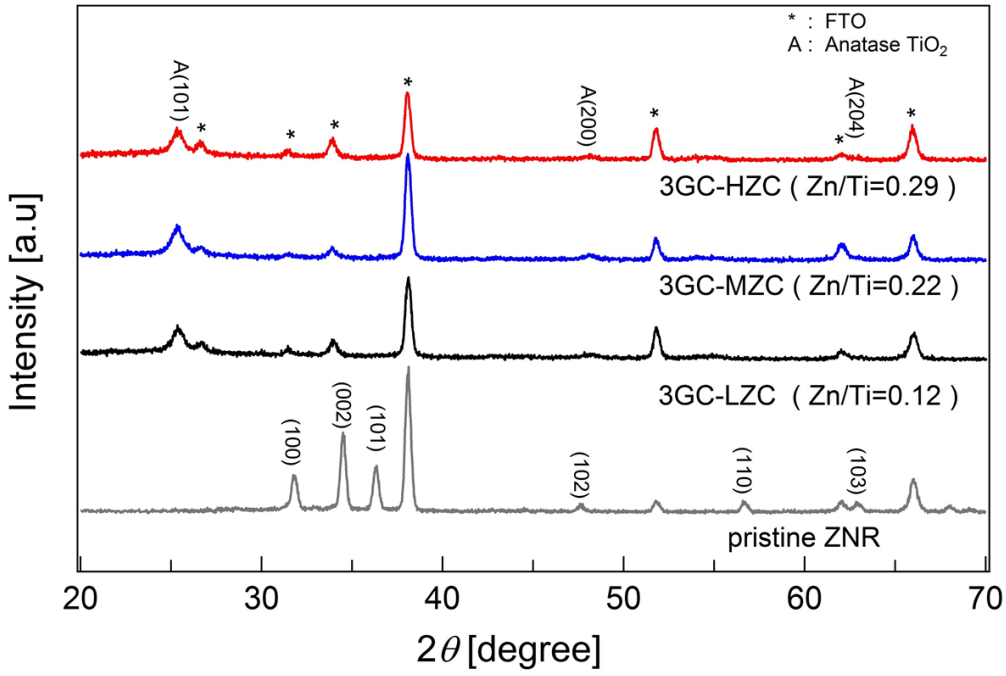

Figure 7 XRD patterns of the TNT arrays of 3GC-HZC, 3GC-MZC, 3GC- LZC, and the pristine ZnO nanorod arrays.

The *I–V* characteristics of the fabricated DSCs with various amounts of surface Zn are shown in Figure 4(b) and the respective photovoltaic data are listed in Table 1. The photovoltaic characteristics exhibited a drastic change with the increase in the amount of Zn on the TNT surface. A V_{OC} value of 0.876 V, which is closer to the ideal maximum of 0.9 V, was achieved for the DSC fabricated with Zn/Ti = 0.29. Such a high V_{OC} value has not been reported with the cells fabricated using typical TiO_2 nanoparticles. The ZnO nanorod/TiO_2 nanoparticles-core/shell structures obtained by changing the conditions of the LPD process are described in reference [35], and an increase of V_{OC} was observed in the ZnO nanorods with the TiO_2-shell. Large variations in both J_{SC} and V_{OC} values were observed in the DSCs prepared using Zn-doped TiO_2 microspheres, as reported in reference [28]. However, the V_{OC} value obtained for the DSC systems fabricated in this study was significantly higher than the values reported in the aforementioned studies. Although it is possible to obtain a remarkably high V_{OC} value from

the current DSC system, the J_{SC} value decreased drastically with the increase in the surface Zn residue.

For further investigation of the influence of the residual Zn, the chemical states of the residual Zn species on the TNT surface were analysed. As the XPS Zn 2p peak showed a very small chemical shift between the Zn^0 and Zn^{2+} contributions, the Zn $L_3M_{45}M_{45}$ Auger electron peaks were used to study the chemical states of Zn [36]. Figure 8 shows the Zn $L_3M_{45}M_{45}$ Auger electron peaks of 3GC-HZC and pristine ZNR excited by the Al K_α X-ray source. The Auger peaks of these samples were located at the same kinetic energy of approximately 988.5 eV. Therefore, the peak of residual Zn is mainly attributed to Zn^{2+}, and thus, the residual Zn species on the TNT surface were principally divalent oxides. From the curve fitting results, the Zn^0 (metal) Auger peak, which is expected to appear at approximately 993.0 eV [36], was in the negligible range. The peaks of Sn $3d_{5/2}$ and $3d_{3/2}$ in 3GC-HZC were obtained from the exposed FTO substrate.

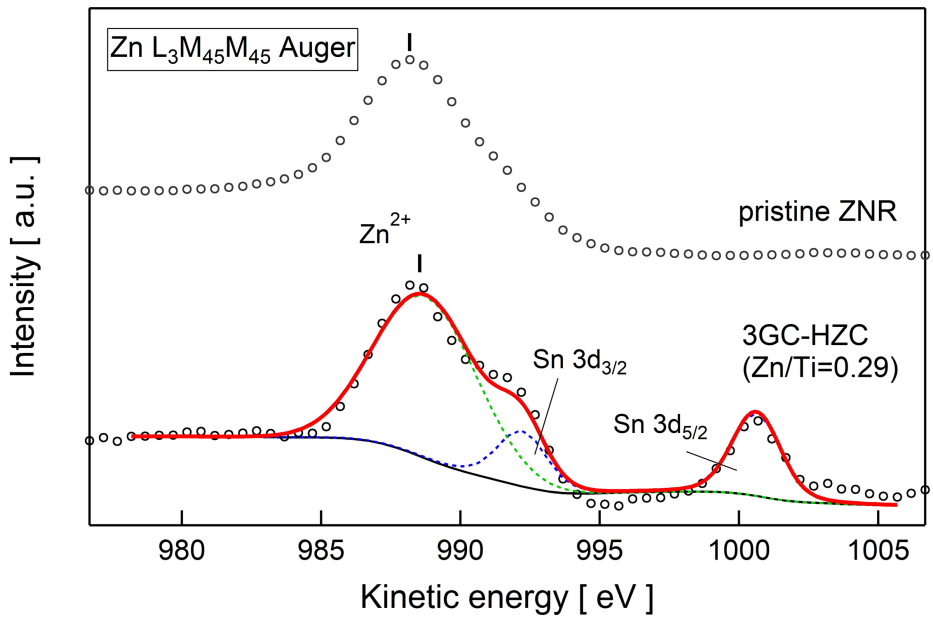

Figure 8 Comparison of XPS Zn $L_3M_{45}M_{45}$ Auger peak of the TNT 3GC-HZC (Zn/Ti=0.29) with pristine ZNR.

As shown in the XPS spectra in Figure 6(b)–(d), the XPS peaks tended to be shifted toward lower binding energy when the amount of Zn residue on the TNT surface increased. The positions of the Zn $2p_{3/2}$ and O 1s peaks of the TNT samples were different from these peak positions of pristine ZNR (Zn $2p_{3/2}$: 1021.61 eV, O1s: 530.33 eV). Moreover, these Zn and O peaks obtained from the TNTs were also different from the peak positions of the ZnO nanoparticles in the ZnO seed layer. The height of the energy barrier (ΔE_C) formed owing to the band bending at the TiO_2/ZnO interface could be estimated using the energy difference between the XPS Zn $2p_{3/2}$ and Ti $2p_{3/2}$ core levels at the TiO_2/ZnO interface, ΔE_{CL}. In our study, ΔE_{CL} had an almost constant value of 563.2 eV, and hence, ΔE_C was also constant. The value of ΔE_{CL} was approximately 0.8 eV larger than that reported in the previous work [37]. From the comparison of the Zn $2p_{3/2}$ and Ti $2p_{3/2}$ peak positions, it was evident that the local structure of the Zn residues was not fully equivalent to the well-crystallised ZnO. Thus, the bond lengths and/or bond angles of the residual Zn on TNT were expected to be different from those of bulk ZnO. As the residual Zn was observed only on the TNT surface, which was confirmed using the Ar-GCIB experiment, local stresses or bond distortions must exist at the Zn sites. The O1s peak of TNT was observed at a lower binding energy side compared to that of stable ZNR and was expected to have a non-stoichiometric structure such as Zn_xO_y ($x < y$).

Three components were observed from the XPS spectrum of O 1s as illustrated in Figure 6(d). The main component at approximately 529.9 eV can be attributed to the lattice oxygen and the shoulder peak at 531.8 eV was assigned to the surface hydroxyl (-OH) group. The other shoulder peak at 530.7 eV was assigned to the surface oxygen defects of Ti-O in some literature [37][38]. However, this peak may exist owing to other factors and may not be solely due to the oxygen vacancy. The atomic concentration of -OH group calculated from the peak area

increased (6.8%, 7.2%, and 8.0%) as the Zn/Ti ratio was increased. Because of active sites near the Zn residue, the surface -OH groups tended to be adsorbed near the sites and became stabilised. The surface -OH groups promoted the adsorption of dye molecules by the reaction with the carboxyl group of N719 dye [39].

Figure 9 shows the band alignment of the TNT with the Zn residue. It has been reported that the differences of the isoelectric points and electron affinity between TiO_2 and ZnO in the TiO_2/ZnO-core/shell structure enhance the open circuit voltage [40]. The electron affinity of ZnO (= 4.15) is smaller than that of TiO_2 (= 4.33) and therefore, the conduction band minimum of ZnO is located at a higher position than that of TiO_2. Moreover, the isoelectric point of ZnO (= 9.5) is larger than that of TiO_2 (= 6.2) [41]. Hence, electrons are easily transferred from ZnO to TiO_2, resulting in an energy barrier in the reverse direction at the ZnO/TiO_2 interface. The energy barrier suppresses the electron leakage to I_3^- in the electrolyte and the quasi-Fermi level is shifted negatively. In this case, the main reason for the enhancement of V_{OC} is the quasi-Fermi level shift owing to the Zn residue on the TNT surface.

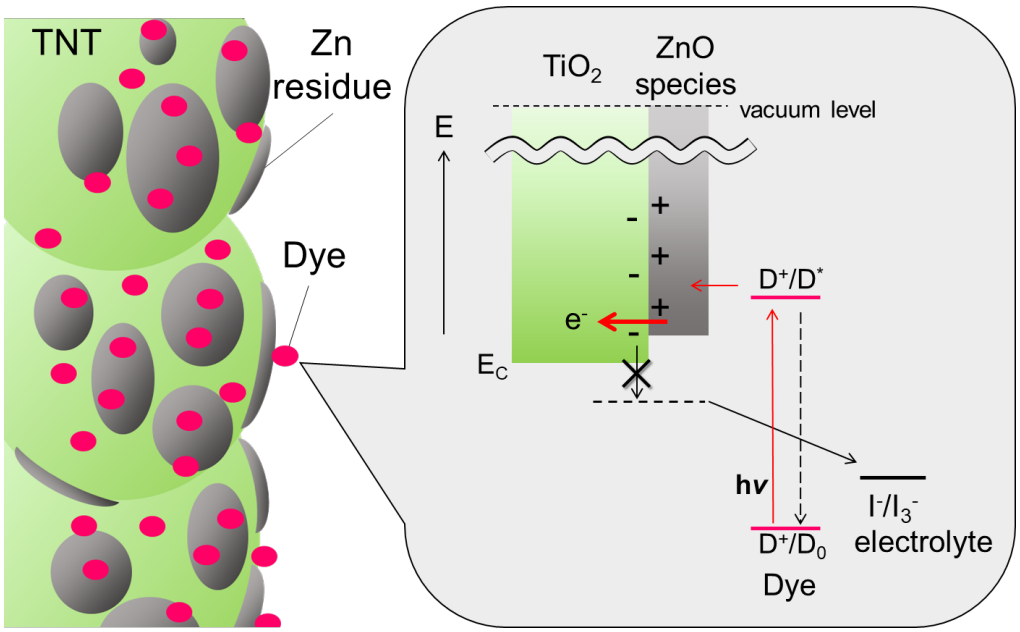

Figure 9 Conduction band alignment of the TiO_2/ZnO species structure owing to the difference between the electron affinity and the isoelectric point of TiO_2 and ZnO. The electron back transfer to I_3^- in the electrolyte can be suppressed owing to the energy barrier at the interface.

Figure 10 shows the UV-Vis absorption spectra of the desorbed dye from the TNT arrays. Slight increase of the absorbance values of the N719 dye and no peak shifts were found for the sample of Zn/Ti = 0.29 as expected from the increase of number of -OH groups at the surface. Therefore, it can be excluded that the dye amount change causes the photocurrent decrease for the high-Zn-amount TNT samples.

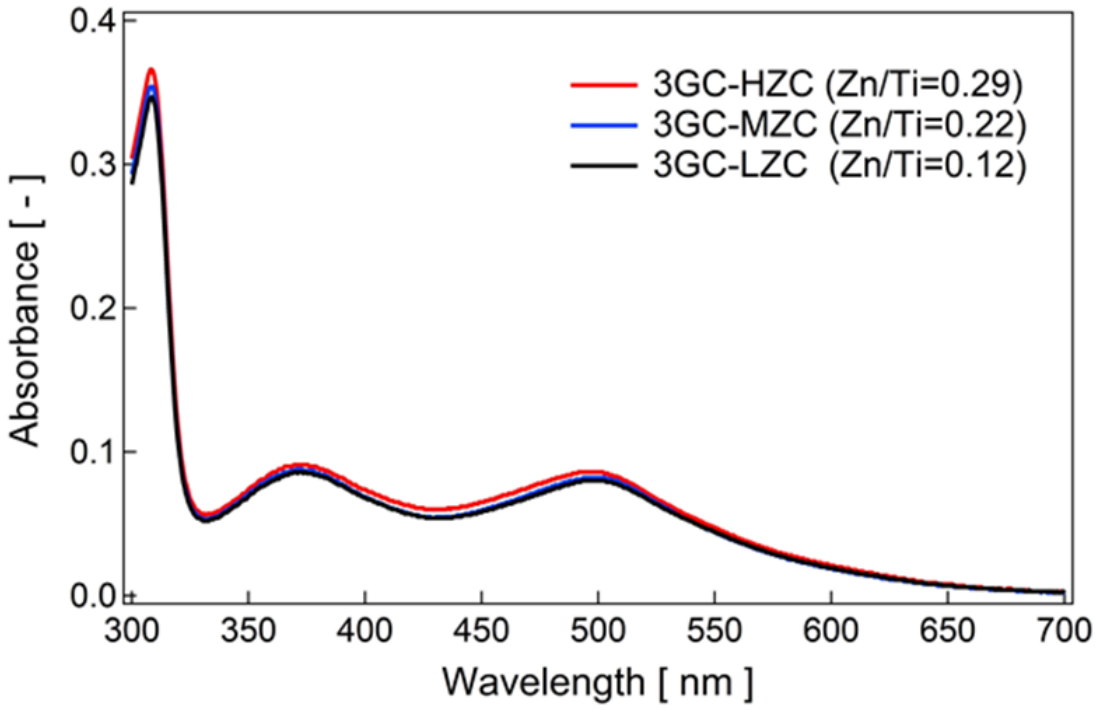

Figure 10 Absorbance spectra of NaOH solution with N719 dye desorbed from the TNT arrays.

It is expected that the main reason for the reduction of J_{SC} is the poor electron injection probability from N719 dye to ZnO species. The N719 is an acidic dye and thus, it can form N719/Zn^{2+} aggregates by reacting with the surface Zn species, thus reducing the dye efficiency [42]. According to the time-dependent density functional theory (TDDFT) calculations, the geometrical overlap with the lowest unoccupied molecular orbital (LUMO) of N719 and the conduction band of ZnO is very small [43]. The photoexcited electrons of N719 dye on ZnO were localised on the bipyridine ligands of the dye, and the electron injection probability from the dye to ZnO was low. Although the amount of dye on the TNT surface was almost same, the electron injection probability was still low, thus reducing J_{SC} drastically.

Another possible reason for reduced J_{SC} is the effect of the electrolyte. 4-tert-butylpyridine (TBP) and Li^+ present in the electrolyte are capable of affecting V_{OC} and J_{SC} significantly [44][45][46]. These effects of TBP and Li^+ varied depending on the difference between the

electrical characteristics, such as carrier density and dielectric constant, of TiO_2 and ZnO [47]. If the amount of Zn residue increases, the effect of TBP and Li^+ is expected to change significantly, but the electrolyte remains adjusted for ideal TiO_2. Therefore, further improvement of photovoltaic performance can be expected by changing the electronic structure of the sensitising dye molecules and adjusting the composition of the electrolyte for the TNT-based DSCs with surface Zn residue.

4. Conclusions

The LPD method was used to fabricate TiO_2 nanotubes, and the length of the nanotubes was controlled successfully by controlling the height of the ZnO nanorod template. TiO_2 nanotube arrays with an average maximum length of 2.8 μm were fabricated, and it was observed that the TiO_2 nanotube was formed with fine particles of 5–15 nm. This is advantageous to dye adsorption owing to its large surface area. DSCs were fabricated by using these TiO_2 nanotube arrays as the photoanode, and a maximum power conversion efficiency of 3.62% was achieved with film thickness of the 2.8 μm TNT arrays. Residual Zn species with the divalent chemical state were observed on the TiO_2 nanotube surfaces, which were a result of the dissolution of ZnO nanorod template. This residual Zn species shifted the quasi–Fermi level of TiO_2 in the negative direction, thus improving open circuit voltage of 0.876 V was successfully achieved, which is close to the theoretical maximum of the TiO_2-based DSCs. For the high Zn amount samples, increase of the number of surface -OH groups on TNT and slight increase of the dye adsorption amount were found. However, the photocurrent of DSCs decreased as the amount of Zn on the surface of TNT. Therefore, it was concluded that injection probability of the photo-excited electrons from adsorbed dye into TNT was significantly decreased by the surface Zn residue.

Acknowledgments

The authors gratefully acknowledge fruitful discussions with Prof. Kenji Murakami, Prof. Akinori Konno, Dr. Shoji Kaneko, and Dr. Takuya Masuda. This research was partially supported by JSPS KAKENHI Grant Number 25390077.

References

[1] B. O'Regan, M. Gratzel, A Low-Cost, High-Efficiency Solar-Cell Based on Dye-Sensitized Colloidal TiO_2 Films, Nature. 353 (1991) 737–740. doi:10.1038/353737a0.

[2] J.M. Kroon, N.J. Bakker, H.J.P. Smit, P. Liska, K.R. Thampi, P. Wang, S.M. Zakeeruddin, M. Grätzel, A. Hinsch, S. Hore, U. Würfel, R. Sastrawan, J.R. Durrant, E. Palomares, H. Pettersson, T. Gruszecki, J. Walter, K. Skupien, G.E. Tulloch, Nanocrystalline dye-sensitized solar cells having maximum performance, Prog. Photovoltaics Res. Appl. 15 (2007) 1–18. doi:10.1002/pip.707.

[3] L.M. Peter, Characterization and modeling of dye-sensitized solar cells, J. Phys. Chem. C. 111 (2007) 6601–6612. doi:10.1021/jp069058b.

[4] K. Park, Q. Zhang, D. Myers, G. Cao, Charge transport properties in TiO_2 network with different particle sizes for dye sensitized solar cells., ACS Appl. Mater. Interfaces. 5 (2013) 1044–52. doi:10.1021/am302781b.

[5] P. Roy, D. Kim, K. Lee, E. Spiecker, P. Schmuki, TiO2 nanotubes and their application in dye-sensitized solar cells, Nanoscale. 2 (2010) 45–59. doi:10.1039/B9NR00131J.

[6] J.R. Jennings, A. Ghicov, L.M. Peter, P. Schmuki, A.B. Walker, Dye-Sensitized Solar Cells Based on Oriented TiO 2 Nanotube Arrays: Transport, Trapping, and Transfer of Electrons, J. Am. Chem. Soc. 130 (2008) 13364–13372. doi:10.1021/ja804852z.

[7] E.V.A. Premalal, N. Dematage, G.R.A. Kumara, R.M.G. Rajapakse, K. Murakami, A. Konno, Shorter nanotubes and finer nanoparticles of TiO2 for increased performance in dye-sensitized solar cells, Electrochim. Acta. 63 (2012) 375–380. doi:10.1016/j.electacta.2011.12.127.

[8] K.P. Kim, S.J. Lee, D.H. Kim, D.K. Hwang, Y.W. Heo, Dye-sensitized solar cells based on trench structured TiO2 nanotubes in Ti substrate, Curr. Appl. Phys. 13 (2013) 795–798. doi:10.1016/j.cap.2012.12.010.

[9] J. Akilavasan, K. Wijeratne, H. Moutinho, M. Al-Jassim, a. R.M. Alamoud, R.M.G. Rajapakse, J. Bandara, Hydrothermally synthesized titania nanotubes as a promising electron transport medium in dye sensitized solar cells exhibiting a record efficiency of 7.6% for 1-D based devices, J. Mater. Chem. A. 1 (2013) 5377. doi:10.1039/c3ta01576a.

[10] B. Liu, E.S. Aydil, Growth of Oriented Single-Crystalline Rutile TiO 2 Nanorods on Transparent Conducting Substrates for Dye-Sensitized Solar Cells, J. Am. Chem. Soc. 131 (2009) 3985–3990. doi:10.1021/ja8078972.

[11] J. Jiu, S. Isoda, F. Wang, M. Adachi, Dye-Sensitized Solar Cells Based on a Single-Crystalline TiO 2 Nanorod Film, J. Phys. Chem. B. 110 (2006) 2087–2092. doi:10.1021/jp055824n.

[12] K. Fujihara, A. Kumar, R. Jose, S. Ramakrishna, S. Uchida, Spray deposition of electrospun TiO 2 nanorods for dye-sensitized solar cell, Nanotechnology. 18 (2007) 365709. doi:10.1088/0957-4484/18/36/365709.

[13] M. Ye, X. Xin, C. Lin, Z. Lin, High efficiency dye-sensitized solar cells based on hierarchically structured nanotubes, Nano Lett. 11 (2011) 3214–3220. doi:10.1021/nl2014845.

[14] G.K. Mor, K. Shankar, M. Paulose, O.K. Varghese, C.A. Grimes, Use of highly-ordered TiO 2 nanotube arrays in dye-sensitized solar cells, Nano Lett. 6 (2006) 215–218. doi:10.1021/nl052099j.

[15] A. Mathew, G.M. Rao, N. Munichandraiah, Enhanced efficiency of tri-layered dye solar cells with hydrothermally synthesized titania nanotubes as light scattering outer layer, Thin Solid Films. 520 (2012) 3581–3586. doi:10.1016/j.tsf.2012.01.002.

[16] D. Gong, C. a. Grimes, O.K. Varghese, W. Hu, R.S. Singh, Z. Chen, E.C. Dickey, Titanium oxide nanotube arrays prepared by anodic oxidation, J. Mater. Res. 16 (2001) 3331–3334. doi:10.1557/JMR.2001.0457.

[17] J. Zhao, X. Wang, R. Chen, L. Li, Fabrication of titanium oxide nanotube arrays by anodic oxidation, Solid State Commun. 134 (2005) 705–710. doi:10.1016/j.ssc.2005.02.028.

[18] B.D. Yao, Y.F. Chan, X.Y. Zhang, W.F. Zhang, Z.Y. Yang, N. Wang, Formation mechanism of TiO2 nanotubes, Appl. Phys. Lett. 82 (2003) 281–283. doi:10.1063/1.1537518.

[19] C.H. Lee, S.W. Rhee, H.W. Choi, Preparation of TiO2 nanotube/nanoparticle composite particles and their applications in dye-sensitized solar cells, Nanoscale Res. Lett. 7 (2012) 48. doi:10.1186/1556-276X-7-48.

[20] K.C. Sun, M.B. Qadir, S.H. Jeong, Hydrothermal synthesis of TiO2 nanotubes and their application as an over-layer for dye-sensitized solar cells, RSC Adv. 4 (2014) 23223. doi:10.1039/c4ra03266g.

[21] J.H. Lee, I.C. Leu, M.C. Hsu, Y.W. Chung, M.H. Hon, Fabrication of aligned TiO2 one-dimensional nanostructured arrays using a one-step templating solution approach, J. Phys. Chem. B. 109 (2005) 13056–13059. doi:10.1021/jp052203l.

[22] K.H. Kim, K. Utashiro, Y. Abe, M. Kawamura, Growth of zinc oxide nanorods using various seed layer annealing temperatures and substrate materials, Int. J. Electrochem. Sci. 9 (2014) 2080–2089.

[23] J. Qiu, X. Li, F. Zhuge, X. Gan, X. Gao, W. He, S.-J. Park, H.-K. Kim, Y.-H. Hwang, Solution-derived 40 μm vertically aligned ZnO nanowire arrays as photoelectrodes in dye-sensitized solar cells, Nanotechnology. 21 (2010) 195602. doi:10.1088/0957-4484/21/19/195602.

[24] L.E. Greene, M. Law, D.H. Tan, M. Montano, J. Goldberger, G. Somorjai, P. Yang, General route to vertical ZnO nanowire arrays using textured ZnO seeds, Nano Lett. 5 (2005) 1231–1236. doi:10.1021/nl050788p.

[25] Y. Zhou, W. Wu, G. Hu, H. Wu, S. Cui, Hydrothermal synthesis of ZnO nanorod arrays with the addition of polyethyleneimine, Mater. Res. Bull. 43 (2008) 2113–2118. doi:10.1016/j.materresbull.2007.09.024.

[26] L.E. Greene, M. Law, J. Goldberger, F. Kim, J.C. Johnson, Y. Zhang, R.J. Saykally, P. Yang, Low-temperature wafer-scale production of ZnO nanowire arrays, Angew. Chemie - Int. Ed. 42 (2003) 3031–3034. doi:10.1002/anie.200351461.

[27] S. Deki, Y. Aoi, O. Hiroi, a Kajinami, Titanium(IV) oxide thin films prepared from aqueous solution, Chem. Lett. (1996) 433–434. doi:10.1246/cl.1996.433.

[28] Y. Zhang, L. Wang, B. Liu, J. Zhai, H. Fan, D. Wang, Y. Lin, T. Xie, Synthesis of Zn-doped TiO2 microspheres with enhanced photovoltaic performance and application for dye-sensitized solar cells, Electrochim. Acta. 56 (2011) 6517–6523. doi:10.1016/j.electacta.2011.04.118.

[29] X. Feng, K. Shankar, M. Paulose, C.A. Grimes, Tantalum-doped titanium dioxide nanowire arrays for dye-sensitized solar cells with high open-circuit voltage, Angew. Chemie - Int. Ed. 48 (2009) 8095–8098. doi:10.1002/anie.200903114.

[30] X. Zhang, S.-T. Wang, Z.-S. Wang, Effect of metal-doping in TiO 2 on fill factor of dye-sensitized solar cells, Appl. Phys. Lett. 99 (2011) 113503. doi:10.1063/1.3635788.

[31] K. Foo, U. Hashim, K. Muhammad, C. Voon, Sol–gel synthesized zinc oxide nanorods and their structural and optical investigation for optoelectronic application, Nanoscale Res. Lett. 9 (2014) 429. doi:10.1186/1556-276X-9-429.

[32] A. Sugunan, H.C. Warad, M. Boman, J. Dutta, Zinc oxide nanowires in chemical bath on seeded substrates: Role of hexamine, J. Sol-Gel Sci. Technol. 39 (2006) 49–56. doi:10.1007/s10971-006-6969-y.

[33] S. Deki, Y. Aoi, Y. Asaoka, A. Kajinami, M. Mizuhata, Monitoring the growth of titanium oxide thin films by the liquid-phase deposition method with a quartz crystal microbalance, J. Mater. Chem. 7 (1997) 733–736. doi:10.1039/a607466i.

[34] C. Xu, P.H. Shin, L. Cao, J. Wu, D. Gao, Ordered TiO2 nanotube arrays on transparent conductive oxide for dye-sensitized solar cells, Chem. Mater. 22 (2010) 143–148. doi:10.1021/cm9027513.

[35] G.K.L. Goh, H.Q. Le, T.J. Huang, B.T.T. Hui, Low temperature grown ZnO@TiO2 core shell nanorod arrays for dye sensitized solar cell application, J. Solid State Chem. 214 (2014) 17–23. doi:10.1016/j.jssc.2013.11.035.

[36] E. Diler, B. Lescop, S. Rioual, G. Nguyen Vien, D. Thierry, B. Rouvellou, Initial formation of corrosion products on pure zinc and MgZn2 examinated by XPS, Corros. Sci. 79 (2014) 83–88. doi:10.1016/j.corsci.2013.10.029.

[37] K. Shen, K. Wu, D. Wang, Band alignment of ultra-thin hetero-structure ZnO/TiO2 junction, Mater. Res. Bull. 51 (2014) 141–144. doi:10.1016/j.materresbull.2013.12.013.

[38] Y. Yu, K. Wu, D. Wang, Dye-sensitized solar cells with modified TiO 2 surface chemical states: The role of Ti 3+, Appl. Phys. Lett. 99 (2011) 192104. doi:10.1063/1.3660711.

[39] K.E. Lee, M.A. Gomez, S. Elouatik, G.P. Demopoulos, Further understanding of the adsorption mechanism of N719 sensitizer on anatase TiO2 films for DSSC applications using vibrational spectroscopy and confocal raman imaging, Langmuir. 26 (2010) 9575–9583. doi:10.1021/la100137u.

[40] Y. Diamant, S. Chappel, S.G. Chen, O. Melamed, A. Zaban, Core-shell nanoporous electrode for dye sensitized solar cells: The effect of shell characteristics on the electronic properties of the electrode, Coord. Chem. Rev. 248 (2004) 1271–1276. doi:10.1016/j.ccr.2004.03.003.

[41] E. Topoglidis, A.E.G. Cass, B. O'Regan, J.R. Durrant, Immobilisation and bioelectrochemistry of proteins on nanoporous TiO2 and ZnO films, J. Electroanal. Chem. 517 (2001) 20–27. doi:10.1016/S0022-0728(01)00673-8.

[42] H.M. Nguyen, R.S. Mane, T. Ganesh, S.H. Han, N. Kim, Aggregation-free ZnO nanocrystals coupled HMP-2 dye of higher extinction coefficient for enhancing energy conversion efficiency, J. Phys. Chem. C. 113 (2009) 9206–9209. doi:10.1021/jp901736w.

[43] J.M. Azpiroz, F. De Angelis, DFT/TDDFT study of the adsorption of N3 and N719 dyes on ZnO(10$\bar{1}$0) surfaces, J. Phys. Chem. A. 118 (2014) 5885–5893. doi:10.1021/jp501058x.

[44] S.E. Koops, B.C. O'Regan, P.R.F. Barnes, J.R. Durrant, Parameters Influencing the Efficiency of Electron Injection in Dye-Sensitized Solar Cells, J. Am. Chem. Soc. 131 (2009) 4808–4818. doi:10.1021/ja8091278.

[45] S.A. Haque, E. Palomares, B.M. Cho, A.N.M. Green, N. Hirata, D.R. Klug, J.R. Durrant, Charge separation versus recombination in dye-sensitized nanocrystalline solar cells: The minimization of kinetic redundancy, J. Am. Chem. Soc. 127 (2005) 3456–3462. doi:10.1021/ja0460357.

[46] X. Yang, S. Zhang, K. Zhang, J. Liu, C. Qin, H. Chen, A. Islam, L. Han, Coordinated shifts of interfacial energy levels: insight into electron injection in highly efficient dye-sensitized solar cells, Energy Environ. Sci. 6 (2013) 3637. doi:10.1039/c3ee42110d.

[47] J. Idígoras, G. Burdziński, J. Karolczak, J. Kubicki, G. Oskam, J. a. Anta, M. Ziółek, The Impact of the Electrical Nature of the Metal Oxide on the Performance in Dye-Sensitized Solar Cells: New Look at Old Paradigms, J. Phys. Chem. C. 119 (2015) 3931–3944. doi:10.1021/jp512330f.